ISTITUTO NAZIONALE DI FISICA NUCLEARE

Sezione di Trieste

INFN/AE-96/04

06 marzo 1996

G. Della Ricca, M. Prest

Simulation of the DELPHI STIC Silicon Shower Maximum Detector

SIS - Pubblicazioni
Laboratori Nazionali di Frascati

Simulation of the DELPHI STIC Silicon Shower Maximum Detector

G. Della Ricca, M. Prest
Dipartimento di Fisica, Università di Trieste and INFN - Sezione di Trieste

Abstract

Shashlik calorimeters have two fundamental limitations: the lack of longitudinal segmentation and a poor e/π separation ability and limited accuracy in the determination of the direction of the showering particle without prohibitive transverse granularity or vertex constraint. To compensate for these limitations the new forward calorimeter of the DELPHI detector has been equipped with two planes of silicon pad detectors respectively after 4 and 7.4 radiation lengths. The novelty of this detector is that to cope with the shashlik readout fibers, the silicon diodes had to incorporate 1.4 mm holes every cm^2. The detector consists of circular strips with radial pitch of 1.7 mm and angular granularity of 22.5°. After a precise simulation of the geometry of the silicon detectors and a careful study of the optimal estimator for the position reconstruction, we have obtained at 45 GeV a radial resolution of (448 ± 6) μm for the 1^{st} plane, of (690 ± 10) μm for the 2^{nd} plane, with which we get an angular resolution of (15.6 ± 0.2) mrad, corresponding to a resolution $\sigma_z < 50$ cm in the determination of the origin z of the particle. The energy resolutions at 45 GeV are 32%, 21% for the two planes. The dependence of these resolutions on the energy is studied. As far as the e/π separation is concerned, given a shower depositing 25 GeV in the calorimeter, for an efficiency in selecting the electrons of 93.4 %, we have obtained a purity greater than 92.0 %.

1 Introduction

1.1 The DELPHI STIC (*Small angle TIle Calorimeter*)

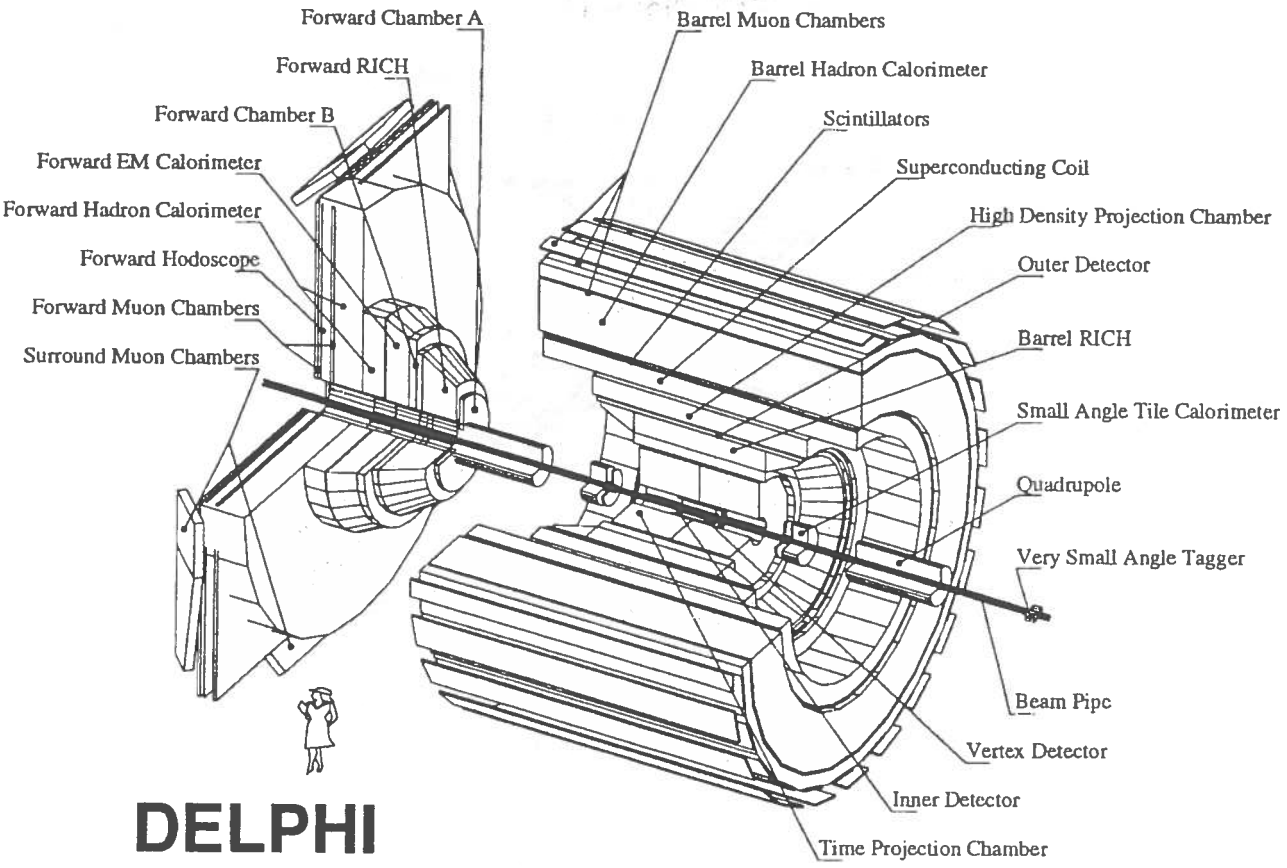

Figure 1: The DELPHI detector

The DELPHI experiment [1] (fig. 1) operating at the LEP collider has installed during the shutdown 1993-94 a new forward calorimeter [2][3][4][5]. The STIC (Small angle TIle Calorimeter) system (fig. 2) consists of two cylinders located symmetrically along the beam axis at 2.20 m from the interaction point. Each cylinder is a sampling calorimeter made of 47 sandwiches of 3.4 mm thick lead plates laminated with 100 μm stainless steel and 3 mm thick scintillator tiles, and two planes equipped with silicon detectors, for a total of $\sim$ 27 radiation lengths. The active volume extends between the radii of 6.5 cm and 42 cm. The signal of the scintillator tiles is read using wavelength-shifter fibres of 1 mm of diameter. A good spatial uniformity is achieved using continuous lead converter and an optimal fiber density ($\sim$ 1 fiber/cm^2) [6]. The calorimeter covers an angular region between 29 and 188 mrad. In fig. 3 planes 1,25 and 49 are shown with the tiles positions. The position of the STIC detector inside the DELPHI experiment is shown in fig. 1.

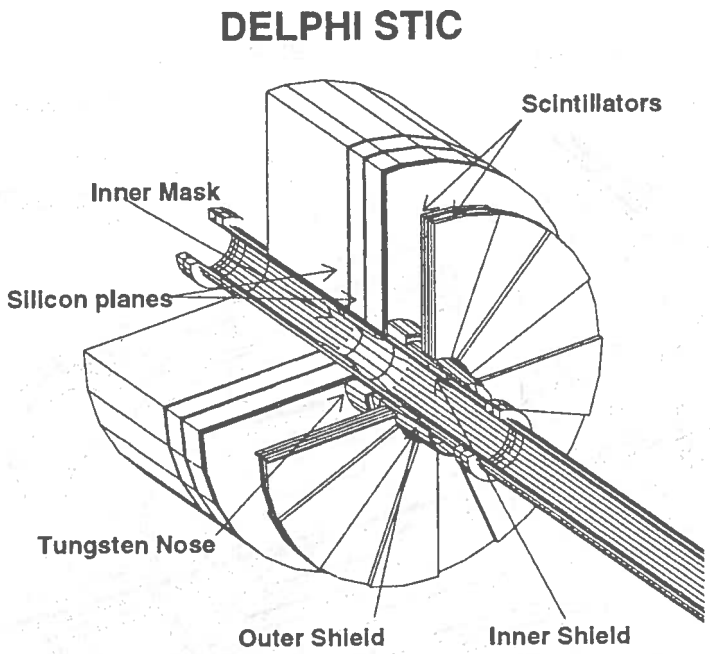

Figure 2: Cut view of STIC

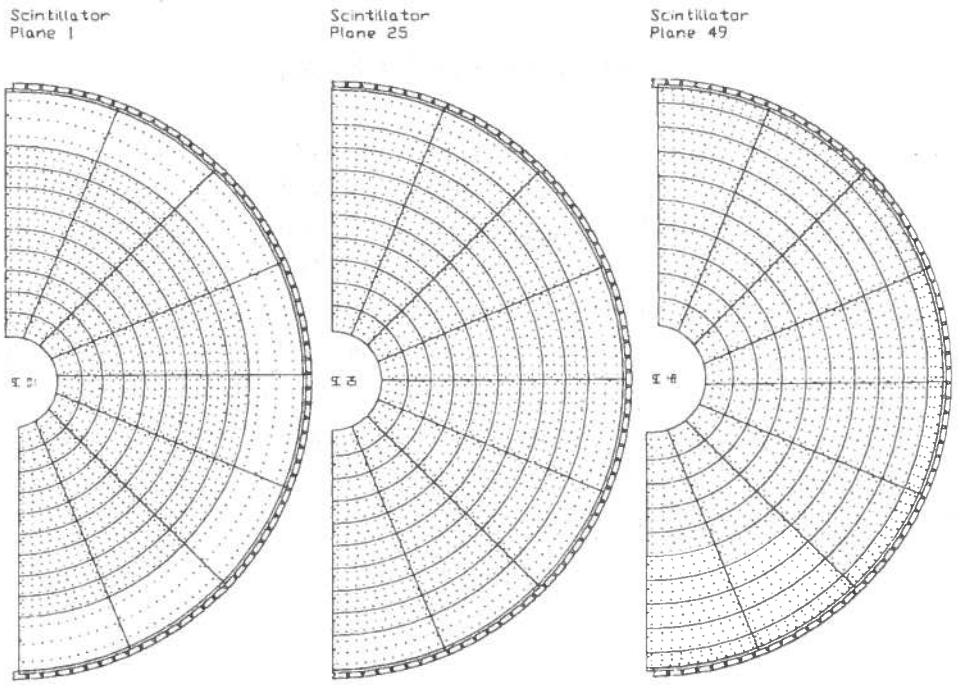

Figure 3: Three different planes of the calorimeter sandwich corresponding to a half module

1.2 The STIC silicon detectors

1.2.1 Why silicon detectors ?

At LEP 200 [7] about the 50% of $q\bar{q}$ events are produced with bremsstrahlung of the initial states, thus reducing the center of mass energy. Reconstructing these events makes it possible to do an "auto-scan" of the total cross-section, between the Z^0 energy and the maximum energy of the machine. The possible studies are:

- ◇ an independent measurement of the neutrino number with a precision of about 1-2%;
- ◇ measurement of α_s for energies between 100 and 200 GeV;
- ◇ measurement of the hadronic to muon cross section ratio $R = \frac{\sigma(e^+e^- \to q\bar{q})}{\sigma(e^+e^- \to \mu^+\mu^-)}$;
- ◇ measurement of anomalous couplings $Z^0Z^0\gamma$.

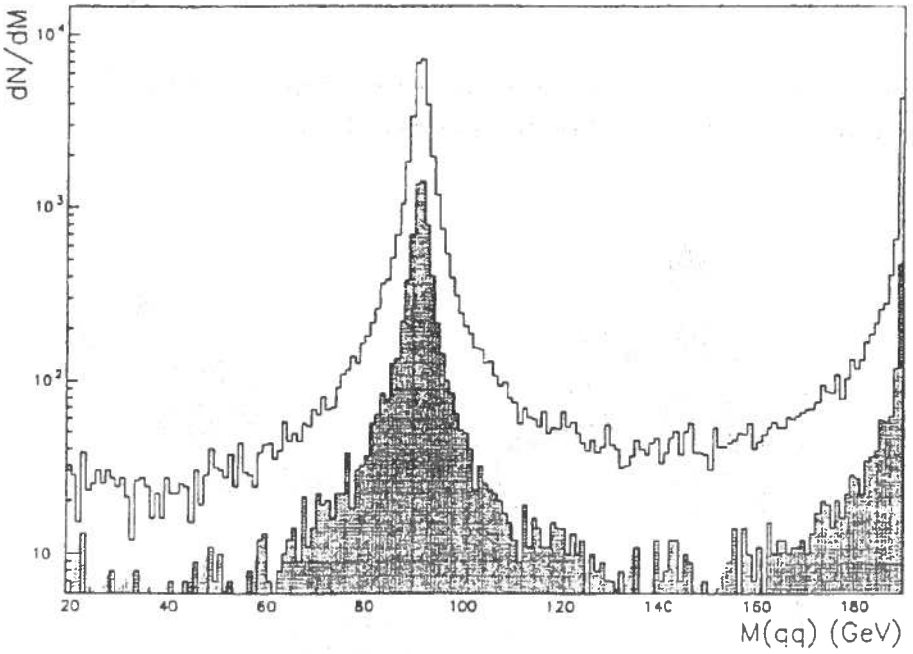

Figure 4: Distribution of the mass of the system $q\bar{q}$ in the reaction $e^+e^- \to q\bar{q}\gamma$ for a center of mass energy of 190 GeV. The shaded area represents the number of events in which the photon falls inside STIC acceptance

Most of the photons are emitted at small angles. About 20% of the events $e^+e^- \to q\bar{q}\gamma$ has a photon inside the minimum STIC acceptance. In fig.4 the mass distribution of the system $q\bar{q}$ is shown: the shaded area represents the events in which the photon falls inside the STIC acceptance.

For these measurements, it is necessary to have an optimal reconstruction of the axis of the electromagnetic shower produced by the photon, to reject the background of off-momentum electrons (caused by interaction with residual gas in the beam pipe), asking that the photon comes from the interaction region (± 0.6 m), and not for example from behind the detector or from the inner region of the calorimeter, close to the beam pipe.

1.2.2 The shower maximum silicon detectors

To improve on STIC limitations (peculiar of shashlik calorimeters), namely the uncertainty in the determination of the shower axis direction and the poor e/π separation, it has been decided to equip the inner region (from

29 to 80 mrad) with two planes of silicon detectors. The two planes have been placed close to the shower maximum (4 and 7.4 radiation length). The positions have been chosen on the basis of simulation results concerning electromagnetic showers in the calorimeter (see par. 2).

1.2.3 Silicon mechanical characteristics

The detectors used are single-sided AC coupled FOXFET [8] silicon strip detectors designed by INFN Torino and Trieste and manufactured by Micron Semiconductor Ltd. [9]. Due to the wavelength-shifter fibers for the calorimeter readout, one of the main features of these silicon detectors is the presence of holes (1.4 mm diameter) to let the fibers go through. A laser beam has been used for the drilling: the precision of the edge cut is about 10 μm. The overall silicon detector geometry has been measured to be precise within 5 μm. The detector thickness is about 300 μm, with an implant and readout strip pitch of 1.712 mm in the first plane and 1.754 mm in the second plane, to match the projective structure of the calorimeter.

For each of the two planes, there are two rows of pads (fig. 5). The first one covers a radial region from 7.15 cm to 11.3 cm with 45° pads subdivided in two sectors with 24 strip each. The second row is made of 22.5° pads with 36 strips each, which extend radially up to 18.03 cm. There are 1920 strips per calorimeter, 3840 in total.

The signal is taken out from the inner region using cables of *Kapton*[1] roughly 35 cm long, which extend up to the surface of STIC where the front end electronics is placed (fig. 6).

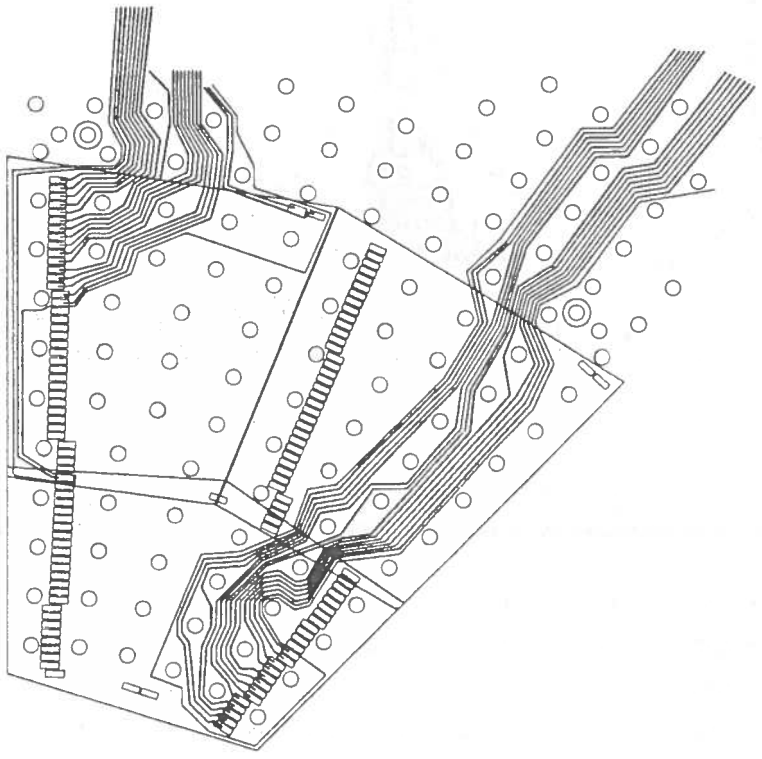

Figure 5: One 45° sector of silicon detectors (the strip structure is not shown)

[1] Gandi's atelier, CERN

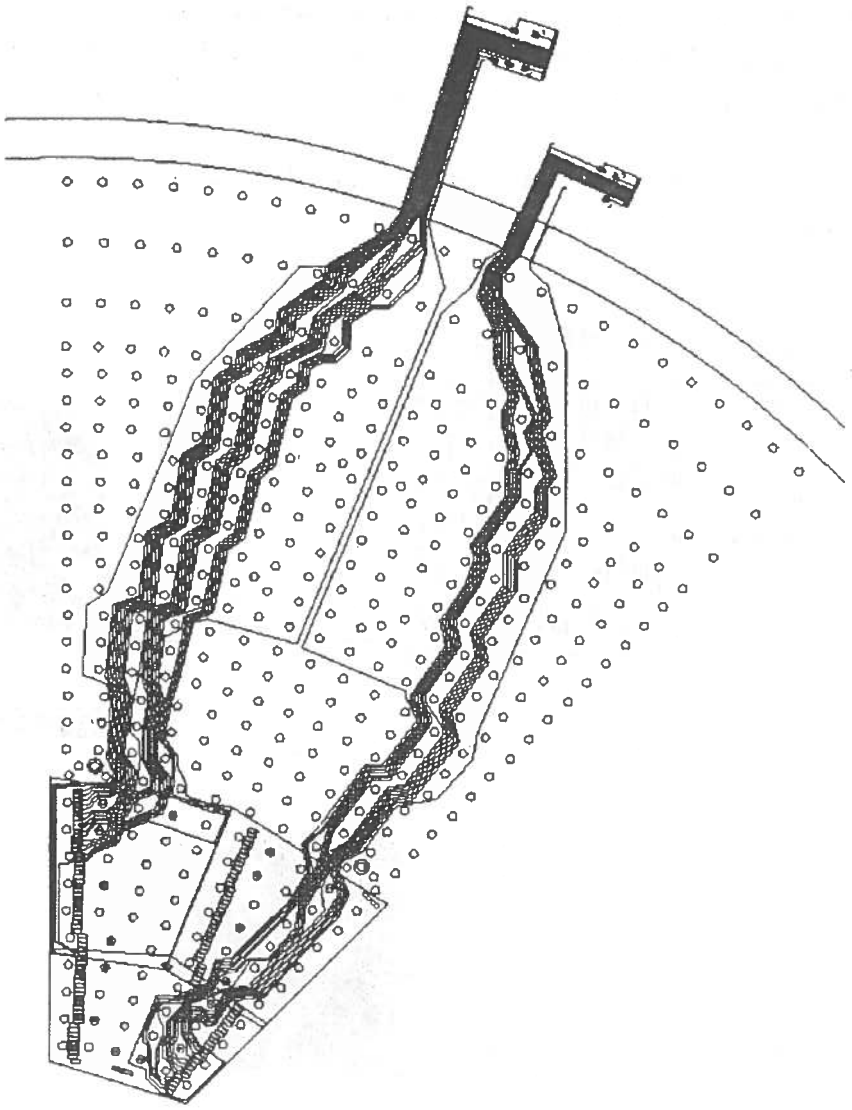

Figure 6: *Kapton* connections for the signal readout

2 The STIC Monte Carlo simulation

The definition and optimization of some of the features of STIC has required the development of a simulation program based on the Monte Carlo method.

2.1 Description of the detector's geometry

For the simulation of the STIC detector [10, 11], the GEANT package (version 3.21) [12] has been chosen because of its capability of describing complex geometries. In fact, it has been possible to reproduce with high precision the geometry of the planes and the position of the wavelength-shifter fibers (see par. 1.1). A special care has been put in describing the beam pipe, its supporting structures and the several tungsten masks (fig. 7).

Once verified that the channelling of particles along the fibers has a negligible effect[1] but increases dramatically the computer time needed for the simulation, it has been decided to use a version without fibres. The effect of the decreasing of the absorbing material due to the presence of holes has been taken into account introducing a special material (*"Sticonium"*) whose characteristics have been obtained averaging the ones of lead, steel and air [10]. In this way the *"Sticonium"* has: atomic number 78.99, atomic weight 199.12, density 11.13 g·cm^{-3}, radiation length 0.582 g·cm^{-2}.

The results have been compared with a simplified version of the geometry developed using the EGS4 code [13]: the shower profiles are in good agreement.

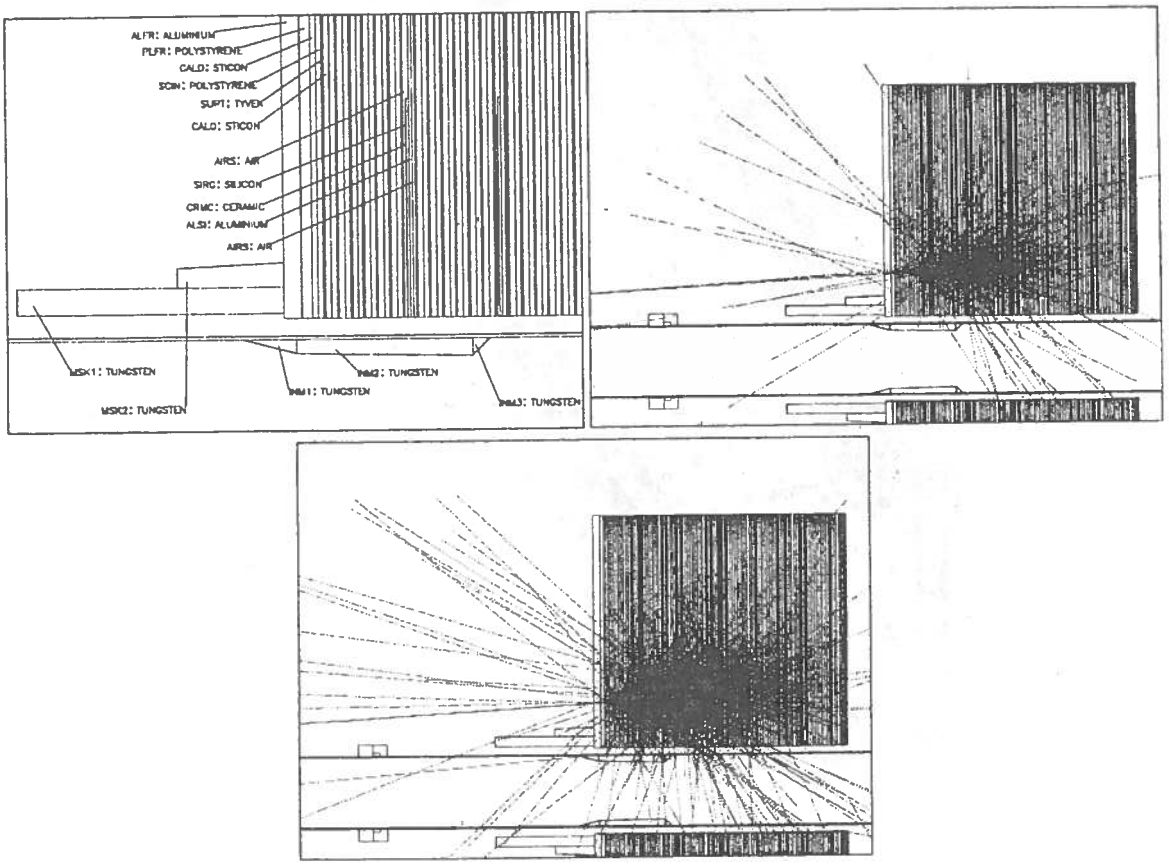

Figure 7: Layout of the calorimeter and examples of electromagnetic showers in STIC

2.2 Results of the simulation of STIC silicon detectors

For the reconstruction of the position of electromagnetic shower center, several algorithms have been studied, all based on the signals collected by the silicon strip. Particular attention has been paid to an eventual *bias*[2] in the reconstruction, since it would influence the precision of the measurement. Before commissioning the silicon detectors, several configurations of the strip planes have been studied, in order to choose the best one. In order to make the simulation as corresponding to reality and as fast as possible, some of the parameters of the models in GEANT have been optimized. In particular, we have studied in detail the effect of the energy thresholds, below which the particles are not tracked any more, and the minimum tracking step.

[1] the fibres are inclined of 3° wrt to the direction of the incident particle

[2] that is the fact that the difference between the expectation value of the estimator and the true value can be different from zero

Not having yet final results on the electronic noise, its effect on the position reconstruction has been studied independently.

2.2.1 A study of different methods of reconstruction of the center of the electromagnetic shower

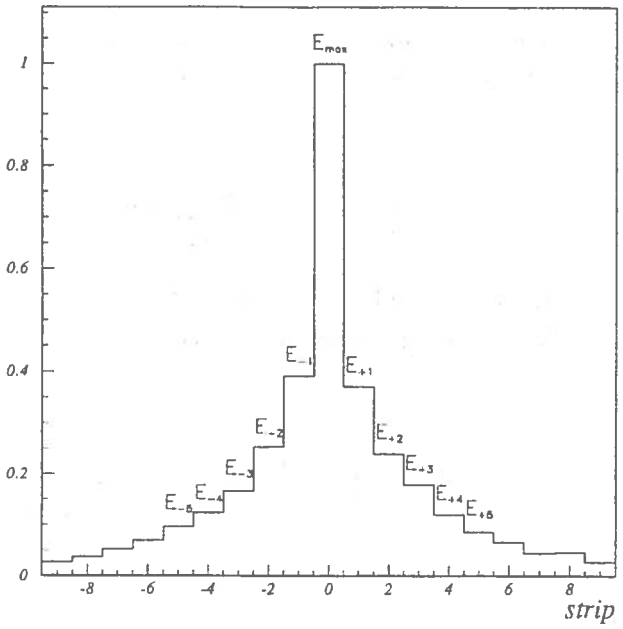

Figure 8: Typical shower profile in one of the STIC silicon detectors

The simplest estimator of the position of the center of an electromagnetic shower is the center of gravity of the signals collected by the silicon strips. For the radial coordinate it is defined as:

$$r_1 = \Delta \frac{\sum_i i E_i}{\sum_i E_i} , \tag{1}$$

where E_i is the signal of the i^{th} strip and Δ is the strip width (1.0 mm, 1.7 mm in these simulations). Anyway, r_1 is a *biased* estimator, because of the exponential shape of the shower profile.

Representing the shower profile with an exponential function with decay constant b [14]:

$$\frac{dE}{dr} \propto \exp^{-\frac{|r-r_{true}|}{b \cdot \Delta}} , \tag{2}$$

it is possible to use, as an estimator of the shower center, a method that takes into account the signals of the two strips sitting on the sides of the strip with the highest signal, through the relation:

$$r_2 = \frac{b \cdot \Delta}{2} \ln \left(\frac{E_{+1}}{E_{-1}} \right) . \tag{3}$$

A third method, based on the hypothesis that the exponential dependence is the same both left and right the central strip, manages to eliminate the parameter b:

$$r_3 = \frac{\Delta}{2} \cdot \frac{\ln (E_{+1}/E_{-1})}{\ln (E_{max}/\min(E_{+1}, E_{-1}))} . \tag{4}$$

To use the second method, it is necessary to know the parameter b, which is connected with the shower

profile. Its value can be computed using the simulation or the real data. It is possible to use methods that start from the data to "auto-calibrate" themselves. Developing this idea, the following algorithm has been found [15]:

1. it is assumed that the shower centers are uniformly distributed on the strip surface, that is:

$$\frac{dN}{dr} = const. \tag{5}$$

This is obviously always possible for simulated data, but it's a good approximation even for real data, since it agrees with the hypothesis that the Bhabha differential cross-section is constant on a strip surface.

2. we build the distribution:

$$\frac{dN}{d\xi}\ ,\ \xi = \frac{\max(E_{-1}, E_{+1})}{E_{max}}\ , \tag{6}$$

where E_{max} is the peak energy (fig. 8) and $E_{\pm 1}$ are the energies of the neighboring strips. The strip with the highest value is chosen because of its smaller relative error.

3. integrating the expression:

$$\frac{dr}{d\xi} = \pm \frac{dN}{d\xi} \cdot \left(\frac{dN}{dr}\right)^{-1}\ ,\ \begin{cases} + & \text{for } E_{+1} > E_{-1} \\ - & \text{for } E_{+1} < E_{-1} \end{cases} \tag{7}$$

we obtain:

$$r_4(\xi') = r_0 \pm \int_0^{\xi'} d\xi \frac{dN}{d\xi} \cdot \left(\frac{dN}{dr}\right)^{-1}\ , \tag{8}$$

where r_0 is the position of the center of the strip with the greatest signal. Considering the value of the constant dN/dr it is found:

$$r_4(\xi') = r_0 \pm \frac{\Delta}{2N_{tot}} \int_0^{\xi'} d\xi \frac{dN}{d\xi}\ , \tag{9}$$

$$\xi' = \frac{\max(E_{-1}, E_{+1})}{E_{max}}\ ,\ \begin{cases} + & \text{for } E_{+1} > E_{-1} \\ - & \text{for } E_{+1} < E_{-1} \end{cases}\ ,$$

where Δ is the width of the strips and N_{tot} is the number of events, simulated or collected.

An algorithm similar to the previous one uses the distribution:

$$\frac{dN}{d\zeta}\ ,\ \zeta = \frac{\min(E_{+1}, E_{-1})}{\max(E_{+1}, E_{-1})}\ , \tag{10}$$

from which we find in a similar way:

$$r_5(\zeta') = r_0 \pm \frac{\Delta}{2N_{tot}} \left(1 - \int_0^{\zeta'} d\zeta \frac{dN}{d\zeta}\right)\ , \tag{11}$$

$$\begin{cases} + & \text{for } E_{+1} > E_{-1} \\ - & \text{for } E_{+1} < E_{-1} \end{cases}$$

In [16], it is suggested to start from the variable:

$$\eta = \frac{\min(E_{max} + 2E_{+1} + E_{+2}, E_{max} + 2E_{-1} + E_{-2})}{\max(E_{max} + 2E_{+1} + E_{+2}, E_{max} + 2E_{-1} + E_{-2})} \ . \tag{12}$$

It is found then:

$$r_6(\eta') = r_0 \pm \frac{\Delta}{2N_{tot}} \left(1 - \int_0^{\eta'} d\eta \frac{dN}{d\eta}\right) \ , \tag{13}$$

$$\begin{cases} + & \text{for } E_{max} + 2E_{+1} + E_{+2} > E_{max} + 2E_{-1} + E_{-2} \\ - & \text{for } E_{max} + 2E_{+1} + E_{+2} < E_{max} + 2E_{-1} + E_{-2} \end{cases} .$$

The results obtained with these several methods in the final layout of the STIC silicon detector are described in tab. 1. For the second method, a value of b had to be found. Instead of deriving it from the transverse profile of the shower, we have decided to compute it minimizing the dispersion of the distribution of the residuals between the true position of the shower center (r_{true}) and the reconstructed one with method 2 (r_2):

$$b_1^{(2)} = (1.5 \pm 0.1) \quad \text{for the } 1^{st} \text{ plane } (4\ X_0)$$
$$b_2^{(2)} = (0.95 \pm 0.03) \quad \text{for the } 2^{nd} \text{ plane } (7.4\ X_0)$$

	1^{st} Plane (4 X_0)	2^{nd} Plane (7.4 X_0)
σ_1	(474 ± 6) μm	(736 ± 11) μm
σ_2	(468 ± 5) μm	(729 ± 11) μm
σ_3	▷ (448 ± 6) μm	(712 ± 10) μm
σ_4	(451 ± 6) μm	(744 ± 11) μm
σ_5	(475 ± 6) μm	(715 ± 10) μm
σ_6	(450 ± 5) μm	▷ (680 ± 10) μm

Table 1: Comparison of different methods of reconstruction of the center of the electromagnetic shower

If these results are compared with the value of the spatial resolution obtained choosing, inside the strip with the highest signal, a value of r uniformly distributed in a random way (that is $\sigma_r \simeq 0.17$ mm$/\sqrt{12} \simeq 490$ μm), it is found that they are worse, at least for middle-low energies (see par. 2.2.5). A detailed study has been done to understand these high values. It has been found, for electrons of 45 GeV, that for 18% of the cases for the 1^{st} plane, and for 35% for the 2^{nd} one, the strip with the highest signal does not contain the center of the electromagnetic shower. The fact is due to the combined effects of the fluctuations in the energy deposit in the silicon detector (the shower is sampled for only 300 μm of thickness) and to the interactions of electrons with the beam pipe: in this last case, even small deviations, due for example to bremsstrahlung, have a high influence on the precision in the reconstruction of the trajectory of the incoming particle. It is a problem with no solution: all the methods we have used are based on the assumption that the strip with the highest signal is the one containing the shower center.

Fig. 9 shows the reconstructed position in the 1^{st} plane as a function of the true one for electrons of 45 GeV. As already said, the method based on the barycenter of the deposited energy is the one with the greatest bias problems. We have chosen the third method of reconstruction for the 1^{st} plane and the sixth method for the 2^{nd} plane. The mean values of the difference between reconstructed and theoretical positions are (5.0 ± 7) μm for the 1^{st} plane and (-7.0 ± 9) μm for the 2^{nd} plane, both compatible with zero. Using the information of the

two planes, it is possible to reconstruct the position of the incoming particle with a precision of about 330 μm.

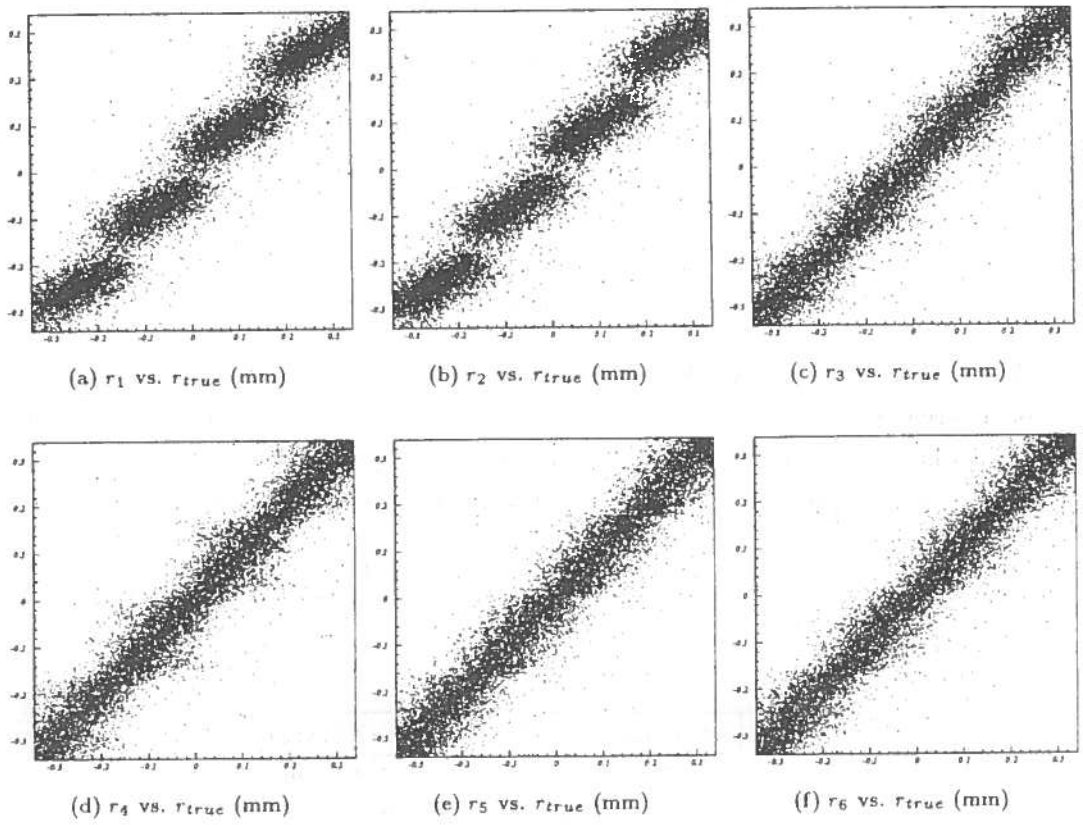

Figure 9: Reconstructed position as a function of true position for the 6 methods studied (1^{st} plane, 45 GeV)

2.2.2 Calibration of the response of the silicon detectors

To study the calibration of the silicon detector response in units of *mip* (*minimum ionizing particle*), 2000 events have been generated, in which a 100 GeV μ meson crosses the calorimeter and the energy deposit in the silicon pads has been measured. In this way, we have obtained the value of energy deposit for these particles, which corresponds to 1 *mip* if the relativistic rise in the Bethe-Bloch curve is disregarded. The distribution is shown in fig. 10, together with a fit to a Landau curve. The most probable value for the energy deposit is

$$(84.6 \pm 0.3) \text{ keV},$$

compatible with the value of about 90 keV found in [17] for 300 μm thick silicon detectors. This value has been used in the following analysis to extract the number of *mip* equivalents to a certain amount of deposited energy. In this way, it is possible to obtain a relative energy scale, which can be used, in combination with the noise level of the electronic chain, to study the spatial resolution of the silicon detectors.

2.2.3 Optimization of the positions of the two planes of silicon detectors

Since the main task of the STIC silicon detectors is the reconstruction of the shower axis rejecting background from off-momentum electrons (see par. 1.2.1), the optimal position of the two planes inside STIC has been studied.

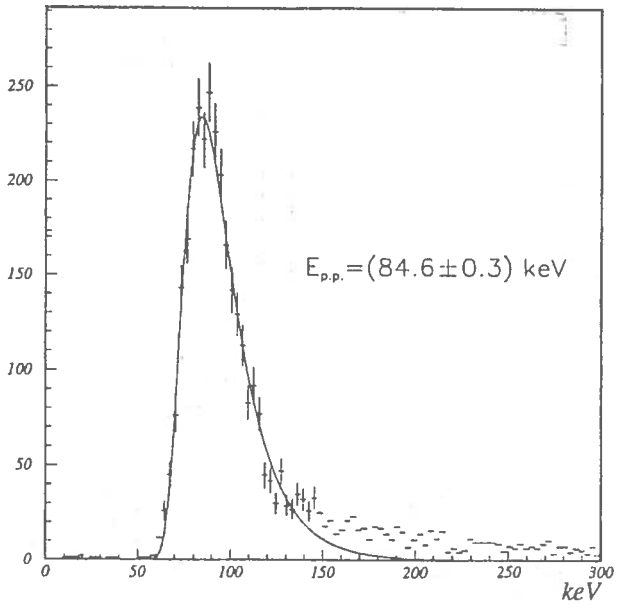

Figure 10: Total energy deposited by μ mesons (45 GeV) in one of the STIC silicon detectors

For each of the configurations listed in tab. 2, 1000 events have been generated and the radial resolution has been measured. The different shower profiles are shown in fig. 11 [18, 19], normalized to the central strip value. Tab. 3 summarizes the results concerning the angular resolution of the two plane system, with the different combinations. We have used the expression:

$$\sigma_\theta = \frac{\sqrt{\sigma_{r_1}^2 + \sigma_{r_2}^2}}{d}\,, \tag{14}$$

where d is the distance between the two planes and σ_{r_1} , σ_{r_2} are respectively the radial resolution of the first and of the second plane.

# Plane	X_0 [g/cm^2]	σ_r [μm]	Signal [*mip*] (central strip)
2	0.57	640 ± 54	8 ± 5
5	2.28	427 ± 13	40 ± 18
8	3.99	449 ± 6	71 ± 21
11	5.70	502 ± 10	75 ± 18
14	7.41	687 ± 17	59 ± 14
17	9.12	1126 ± 31	41 ± 13

Table 2: Radial resolution for different positions of the silicon detectors

The choice of the optimal configuration has been done keeping in mind:

- the number of *mips* collected by the strip with the highest signal and the expected noise of the electronic chain;
- the radial resolution of the two planes;
- the angular resolution.

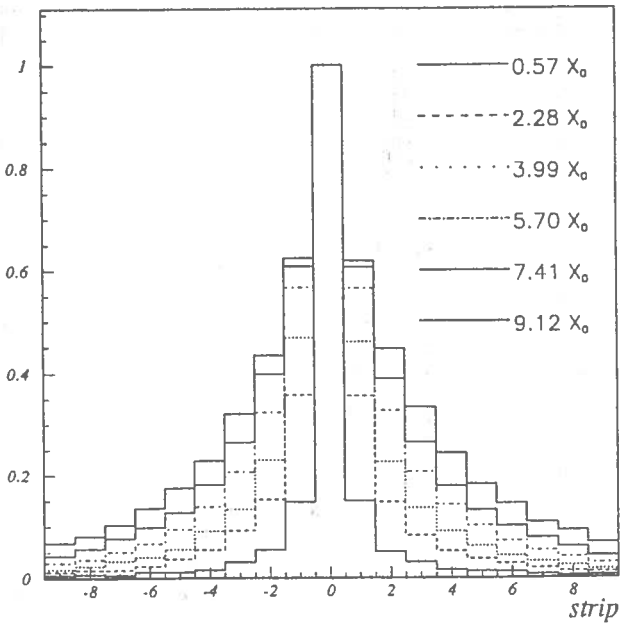

Figure 11: Trasverse profile of the electromagnetic shower produced by a 45 GeV electron as a function of depth

♯ Plane	2	5	8	11	14	17
2	···	43.6	21.6	14.5	10.4	11.3
5	43.6	···	31.1	15.7	12.0	12.0
8	21.6	31.1	···	30.7	17.6	15.8
11	14.5	15.7	30.7	···	35.4	23.8
14	10.4	12.0	17.6	35.4	···	50.6
17	11.3	12.0	15.8	23.8	50.6	···

Table 3: Angular resolution in mrad for different positions of the silicon detectors

It has been decided to put one plane in position 8 (after 4 X_0) and one in position 15 (after 7.4 X_0). With this choice the radial and angular resolutions are:

$$\begin{cases} \sigma_{r_1} = (448 \pm 6)\ \mu\text{m} \\ \sigma_{r_1} = (690 \pm 10)\ \mu\text{m} \\ \sigma_{\theta_{12}} = (15.6 \pm 0.2)\ \text{mrad} \end{cases} \tag{15}$$

Using the position r of the impact point of the particle on the calorimeter and its incidence angle θ (computed using the information of the silicon detectors) it is possible to find the error on the determination of the origin z of the particle, defined as the intersection of its trajectory with the beam axis:

$$z = \frac{r}{\tan\theta}\ , \tag{16}$$

We find:

$$\sigma_z \simeq \frac{r}{\sin^2\theta} \cdot \sigma_\theta\ , \tag{17}$$

from where, if $\theta \in [30, 80]$ mrad, $\sigma_z < 0.5$ m. This resolution is enough to distinguish particles coming from the interaction point from background of off-momentum electrons.

2.2.4 A study of the dependence of the radial resolution from the width of the strips

We have studied two different layouts:

1. strips of 1.0 mm (0.9 mm active region);
2. strips of 1.7 mm (1.6 mm active region).

The obtained radial resolutions are listed in tab. 4.

	Strips of 1.0 mm	Strips of 1.7 mm
$\sigma_r(1^{st}$ plane)	$(427 \pm 11)\mu$m	$(448 \pm 6)\mu$m
$\sigma_r(2^{nd}$ plane)	$(858 \pm 40)\mu$m	$(690 \pm 10)\mu$m

Table 4: Effect of the strip width on the radial resolution

The effect of the non-correspondence between the strip with the maximum signal and the one hit by the trajectory of the incoming electron is more evident, especially in the second plane, using strips of 1.0 mm pitch. Only in 28% of the cases for the 1^{st} plane, 15% for the 2^{nd} one, the identification is correct. Mechanical problems concerning the holes for the fibres have required strips of 1.7 mm. Simulation results agree with this choice.

2.2.5 Energy dependence of the radial resolution

The radial resolutions obtained for different energies of the incoming electron are listed in tab. 5.

E [GeV]	σ_{r_1} [μm]	σ_{r_2} [μm]
5	2900 ± 100	4400 ± 200
15	980 ± 30	1700 ± 60
25	640 ± 20	1150 ± 40
35	520 ± 15	860 ± 30
45	448 ± 6	690 ± 10
65	340 ± 9	540 ± 17
85	300 ± 8	420 ± 10

Table 5: Radial resolution as a function of the generated electron energy

In fig. 12 it is shown the dependence $\sigma_r \propto 1/\sqrt{E}$ of the spatial resolution, related to the fluctuations in the energy deposit in the silicon detectors.

We find:

$$\begin{cases} \sigma_{r_1} = (4.1 \pm 0.1)/\sqrt{E} + (-0.15 \pm 0.02) \text{ mm} \\ \sigma_{r_2} = (7.6 \pm 0.2)/\sqrt{E} + (-0.41 \pm 0.03) \text{ mm} \\ \sigma_\theta = (161 \pm 4)/\sqrt{E} + (-7.9 \pm 0.6) \text{ mrad} , \end{cases} \tag{18}$$

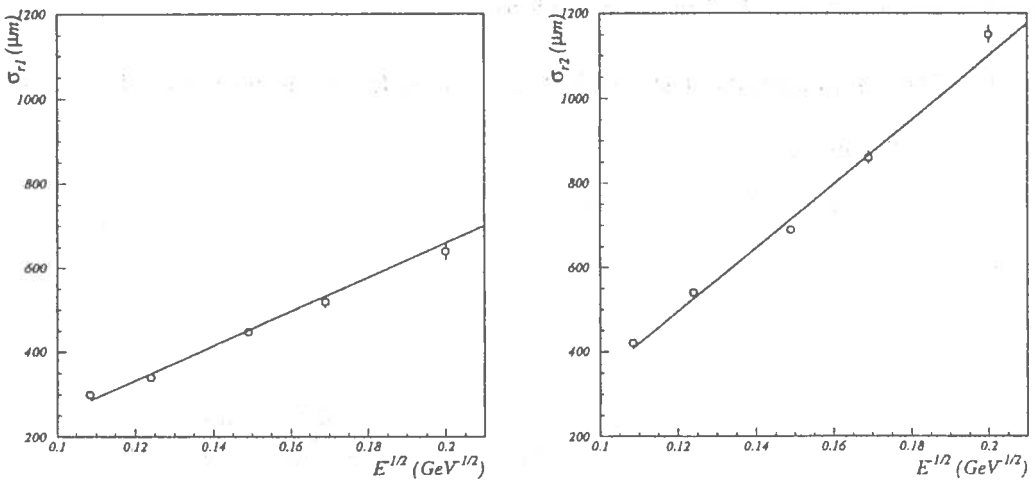

Figure 12: Radial resolution as a function of $E^{-1/2}$ for the 1^{st} and 2^{nd} plane

with E expressed in GeV. The variation of the shower profile as a function of E is shown in fig. 13 (the shower profiles are normalized to the central strip value).

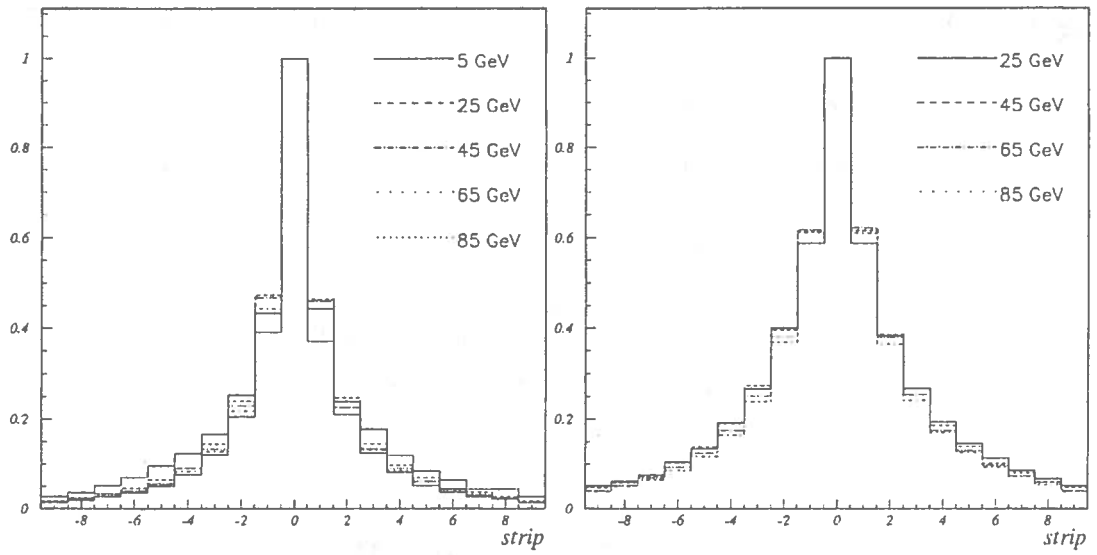

Figure 13: Trasverse profile of the shower as a function of the energy of the incoming electron for the 1^{st} and 2^{nd} plane

2.2.6 Energy resolution and linearity

The energy resolutions obtained for different energies of the incoming electron are listed in tab. 6.

E [GeV]	*mip*-equiv. 1^{st} Plane (total energy)	*mip*-equiv. 2^{nd} Plane (total energy)	*mip*-equiv. 1^{st} Plane (central strip)	*mip*-equiv. 2^{nd} Plane (central strip)
5	49 ± 18	51 ± 15	11 ± 4	8 ± 3
15	121 ± 37	128 ± 29	27 ± 8	20 ± 6
25	176 ± 51	217 ± 39	41 ± 12	32 ± 8
35	225 ± 62	313 ± 50	54 ± 16	47 ± 11
45	270 ± 82	401 ± 59	68 ± 20	60 ± 13
65	359 ± 110	579 ± 70	91 ± 26	88 ± 19
85	420 ± 126	745 ± 95	112 ± 33	119 ± 21

Table 6: Energy deposit as a function of the generated electron energy

In fig. 14 it is shown the energy resolution as a function of the simulated particle energy.

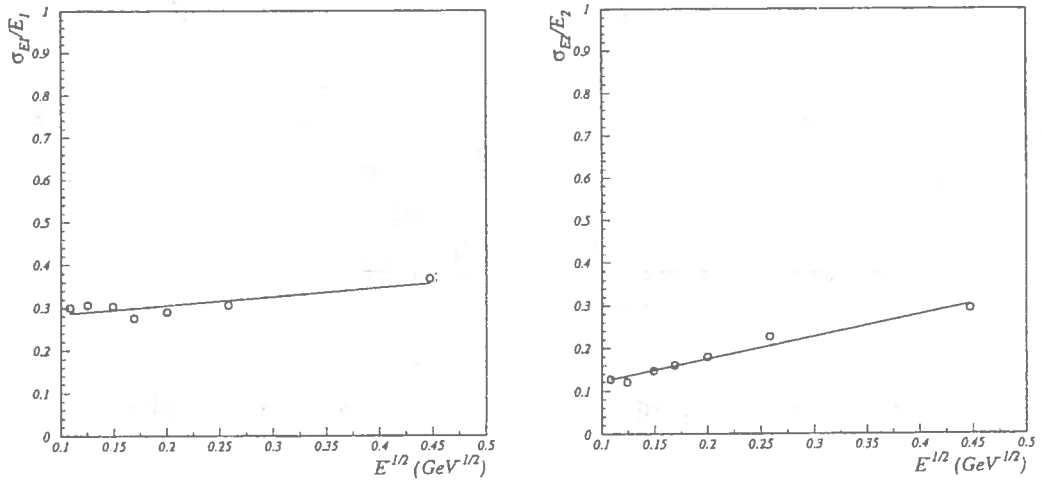

Figure 14: Energy resolution as a function of $E^{-1/2}$ for the 1^{st} and 2^{nd} plane

We find:

$$\begin{cases} \sigma_{E_1}/E_1 = (20.4 \pm 3.5)/\sqrt{E} + (26.5 \pm 0.8)\ \% \\ \sigma_{E_2}/E_2 = (52.1 \pm 3.5)/\sqrt{E} + (7.1 \pm 0.8)\ \% \end{cases} \tag{19}$$

where E_1 (E_2) is the energy deposit in the 1^{st} (2^{nd}) plane expressed in *mips* and E is the energy of the shower in GeV. The first term is the usual dependence $\sigma_E/E \propto 1/\sqrt{E}$ of the energy resolution, related to the fluctuations in the energy deposit in the silicon detectors, the second one represents the fluctuations in the shower starting point, which are more evident in the 1^{st} plane.

The longitudinal shower shape in a sampling calorimeter can be parametrized using the well known Γ-

distribution for the energy release dE/dt as a function of the shower depth $t[X_0]$ [20]:

$$\frac{dE}{dt} = E\frac{b^{\alpha+1}t^{\alpha}e^{-\beta t}}{\Gamma(\alpha+1)} \tag{20}$$

where E is the shower energy and α, β are empirical parameters, functions of the initial energy E. Given this equation, we have obtained that the dependence of the energy deposit on the energy of the shower can be parametrized as:

$$\begin{cases} E_1 = (12.52 \pm 0.19)E + (-1.70 \pm 0.04)E\log E + (0.3 \pm 1.4)\ mip \\ E_2 = (8.94 \pm 0.14)E + (-0.03 \pm 0.03)E\log E + (1.5 \pm 1.1)\ mip \end{cases} \tag{21}$$

with E_1, E_2 expressed in *mips* and E in GeV.

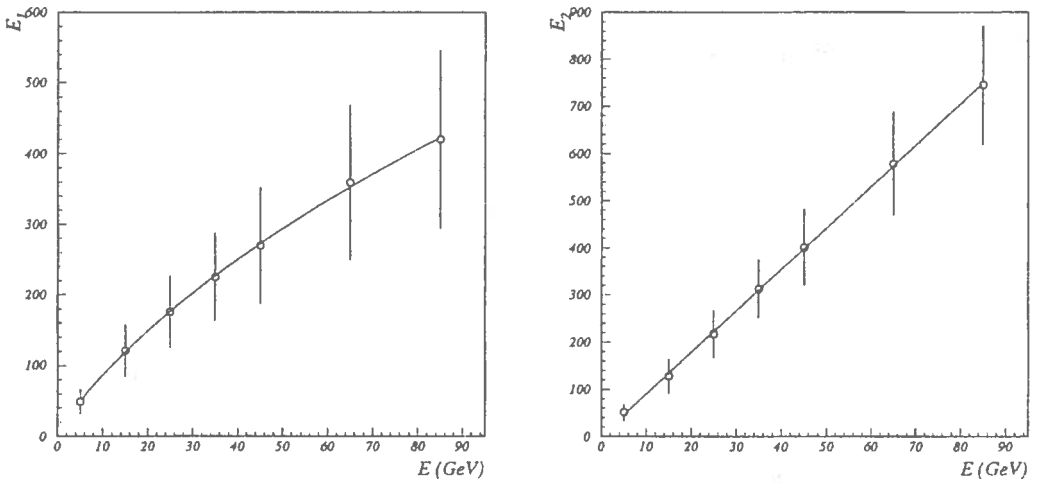

Figure 15: Energy deposit as a function of E for the 1^{st} and 2^{nd} plane

2.2.7 Electron/pion separation

Given a shower depositing an energy E in the STIC detector, we have studied a method to separate electromagnetic showers from hadronic ones. We have decided to use, as discriminating variables, E_1 (E_2) and N_1 (N_2), respectively the energy deposit and the number of strips with signal above a given threshold in the 1^{st} (2^{nd}) plane of the silicon detectors. We have developed a series of cuts on these variables, depending on the energy E.

For each value of E reported in tab. 7 we have applied these cuts to a sample of showers, containing events produced by an equal number of electrons (of energy E) and pions (of energy E_π, with $E_\pi \leq E$).

We have tuned the cuts in order to select a sub-sample of events enriched in the number of electrons. In tab. 7 the efficiency and the purity for electrons are reported as a function of the deposited energy E and of the energy E_π of the pion.

For example, given a shower depositing 25 GeV in the calorimeter, for an efficiency in selecting the electrons of 93.4 %, the purity is greater than 92.0 %.

E	$E_\pi = 15$ GeV		$E_\pi = 25$ GeV		$E_\pi = 35$ GeV		$E_\pi = 45$ GeV	
[GeV]	*Eff.*	*Pur.*	*Eff.*	*Pur.*	*Eff.*	*Pur.*	*Eff.*	*Pur.*
5	88.4 ± 3.1	93.6 ± 2.6	96.8 ± 3.2	92.3 ± 3.4	66.8 ± 3.2	93.0 ± 4.0	66.8 ± 3.2	91.2 ± 6.3
15	95.1 ± 3.2	43.5 ± 7.9	95.1 ± 3.2	87.1 ± 2.7	95.1 ± 3.2	92.1 ± 3.0	95.1 ± 3.2	92.9 ± 4.6
25	–	–	89.5 ± 3.1	31.3 ± 9.9	77.7 ± 2.9	94.1 ± 4.0	77.7 ± 2.9	97.1 ± 5.3
35	–	–	–	–	84.2 ± 3.0	36.7 ± 11.1	84.2 ± 3.0	26.7 ± 9.4
45	–	–	–	–	–	–	97.1 ± 1.4	00.0 ± 0.0

Table 7: Efficiency and purity as a function of the energy E detected in the calorimeter

2.2.8 Effects of the magnetic field

Once in DELPHI, STIC will be in a magnetic field of 1.2 T, directed along z. The effect on the shower development has been studied [21].

	$B_z = 0.0$ T	$B_z = 1.2$ T
$E_{tot}(1^{st}$ plane)	(270 ± 82) *mip*	(274 ± 75) *mip*
$E_{tot}(2^{nd}$ plane)	(401 ± 59) *mip*	(401 ± 59) *mip*
$E_{max}(1^{st}$ plane)	(68 ± 20) *mip*	(69 ± 20) *mip*
$E_{max}(2^{nd}$ plane)	(60 ± 13) *mip*	(61 ± 14) *mip*
$\sigma_r(1^{st}$ plane)	$(405 \pm 7)\mu$m	$(448 \pm 6)\mu$m
$\sigma_r(2^{nd}$ plane)	$(699 \pm 13)\mu$m	$(690 \pm 10)\mu$m

Table 8: Effects of the DELPHI magnetic field on some characteristic quantities of the electromagnetic shower and on the radial resolution

A magnetic field along the shower axis should have a focusing effect that counterbalances multiple scattering. An orthogonal component should cause an enlargement of the shower. We have generated two event samples, one with $B_z = 0.0$ T and one with $B_z = 1.2$ T. No dependence from B_z has been observed (see fig. 16): the contribution of the multiple scattering is dominant. In tab. 8 the results of the effect of the magnetic field on the spatial resolution are reported. For the 1^{st} plane the resolution seems better in absence of the magnetic field. For the 2^{nd} plane no appreciable variations are present.

2.2.9 Effects of the electronic noise

We have studied the effect of the electronic noise on the radial resolution. We have added to the signal a gaussian noise, proportional to the energy deposited by a *mip* in the silicon detector planes ($\simeq 84.6$ keV). The results are listed in tab. 9.

It is evident how till a noise level equivalent to 2-3 *mips*, the resolution is not altered. In the final configuration, we expect a noise value of about 0.25-1.0 *mip* per channel.

2.3 Optimization of some parameters of the simulation

2.3.1 Energy thresholds

We have studied in detail the effects of different values of the energy thresholds for the tracking of electrons and photons.

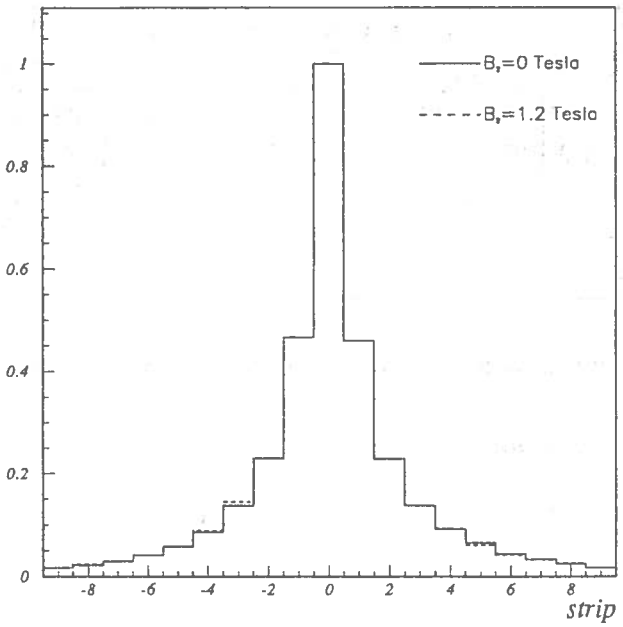

Figure 16: Trasverse profiles of the shower for $B_z = 0$ T and $B_z = 1.2$ T in the 1^{st} plane

$\sharp$ *mip*	$\sigma_r(1^{st}$ plane) [μm]	$\sigma_r(2^{nd}$ plane) [μm]	σ_θ [mrad]
0	448 $\pm$ 6	690 $\pm$ 10	15.6 $\pm$ 0.2
0.5	449 $\pm$ 6	691 $\pm$ 10	15.6 $\pm$ 0.2
1	451 $\pm$ 6	702 $\pm$ 10	15.8 $\pm$ 0.2
2	455 $\pm$ 6	712 $\pm$ 10	16.0 $\pm$ 0.3
5	484 $\pm$ 7	766 $\pm$ 11	17.1 $\pm$ 0.3
10	566 $\pm$ 8	910 $\pm$ 16	20.3 $\pm$ 0.3

Table 9: Effect of the electronic noise on the radial resolution

We have checked that in the interval 10 keV-200 keV, there are no evident differences as far as: mean energy deposit, energy dispersion, transversal shower profiles measured by the strips (tab. 10). We have also observed that there is a linear relation between the energy of the shower and the CPU time spent for its simulation ($\approx$ 1.3 s/GeV for an energy threshold of 100 keV) on an ALPHA DEC 3000-M800.

2.3.2 Tracking

One of the main problems for the particle tracking is the crossing of separation surfaces between different materials [21]. If there's no magnetic field and the incidence angle of the track is big, the situation is easy. But if the particle gets nearer the surface almost parallel to it, there are some difficulties: the multiple scattering can take it out of the material. If there's a magnetic field, the situation is even worse. The usual method accounts for a tracking done with small steps and for a test to check if the material has changed. If the step is too big, the particle can cross thin layers of materials enclosed in bigger volumes. This can be avoided optimizing the step value as a function of the material. For silicon detectors the maximum step must be of the order of the wafer thickness, that is about 300 μm. To avoid infinite computer time, it is possible to enclose the silicon planes in a bigger volume, where tracking is done very accurately. For the STIC silicon detectors we have used

Energy threshold [keV]	$\sigma_r(1^{st}$ plane) [μm]	$\sigma_r(2^{nd}$ plane) [μm]
10	413 ± 6	566 ± 8
50	410 ± 10	572 ± 15
100	383 ± 10	568 ± 17
150	402 ± 11	567 ± 17
200	390 ± 10	522 ± 14

Table 10: Energy threshold dependence of the radial resolution

the fact that the detectors themselves and the supports are positioned inside a volume of air. The step used is 10 μm. Tab. 11 shows the results obtained with the reduced step and with the standard GEANT one.

	Standard step in the volume containing the planes of silicon ($\gg 300$ μm)	Reduced step in the volume containing the planes of silicon (10 μm)
$E_{tot}(1^{st}$ plane)	(270 ± 82) *mip*	(270 ± 82) *mip*
$E_{tot}(2^{nd}$ plane)	(401 ± 59) *mip*	(401 ± 59) *mip*
$E_{max}(1^{st}$ plane)	(68 ± 20) *mip*	(68 ± 20) *mip*
$E_{max}(2^{nd}$ plane)	(60 ± 13) *mip*	(60 ± 13) *mip*
$\sigma_r(1^{st}$ plane)	$(448 \pm 6)\mu$m	$(459 \pm 6)\mu$m
$\sigma_r(2^{nd}$ plane)	$(690 \pm 10)\mu$m	$(690 \pm 10)\mu$m

Table 11: Effect of the maximum step allowed for the tracking on some characteristic quantities of the electromagnetic shower and on the radial resolution

No visible differences have been observed, probably because the great number[1] of particles present in the shower smears out the effect.

3 Conclusions

Using the GEANT package, a precise description of the STIC detector has been obtained. The geometry of the two planes of silicon detectors has been reproduced. We have studied several algorithms for the position reconstruction of the electromagnetic shower center, based on the signals collected by the silicon strips. We have obtained a radial resolution at 45 GeV of (448 ± 6) μm for the 1^{st} plane, of (690 ± 10) μm for the 2^{nd} plane, and thus an angular resolution of (15.6 ± 0.2) mrad, corresponding to a resolution $\sigma_z < 1$ m in the determination of the origin z of the particle, good enough to reject off-momentum electron background. The energy resolutions at 45 GeV are 32%, 21% for the two planes. These results were used to decide the final configuration of the planes, before the commissioning of the silicon detectors. As far as the e/π separation is concerned, given a shower depositing 25 GeV in the calorimeter, for an efficiency in selecting the electrons of 93.4 %, we have obtained a purity greater than 92.0 %.

[1] $\approx$ 700 around the shower maximum at 45 GeV in Rossi's B-Approximation [22]

Acknowledgements

We express our appreciation particularly to Paolo Poropat for many critical discussions and support, as well as to Erik Vallazza for his encouragement during this work. We thank Maurizio Bonesini for the central role he played in the development of the Monte Carlo program. Finally, we want to thank the INFN Trieste and CERN laboratories for their support, which has made possible the present analysis.

Contents

List of Figures

List of Tables

References

[1] P. Aarnio et al., The DELPHI Detector at LEP, NIM A303 (1991) 233 – 276.

[2] DELPHI collaboration, Proposal for the Replacement of the Small Angle Calorimeter of DELPHI, CERN/LEPC/92-6, 1992;
DELPHI collaboration, Proposal for the Upgrade of DELPHI in the Forward Region, CERN/LEPC/92-13/P2 Add2, 1992;
DELPHI collaboration, DELPHI Status Report and Proposal of the Upgrade in the Forward Region, DELPHI 92-155 GEN 136, 1992;

[3] A.C. Benvenuti et al.,Prototype Design, Construction and Test of a Pb/Scintillator Sampling Calorimeter with Wavelength Shifter Fiber Optic Readout, IEEE Trans. Nucl. Sci. 40 (1993) 537-545

[4] A.C. Benvenuti et al., Status of the DELPHI Small Angle Tile Calorimeter Project, presented by V. Obraztsov, contribution to the Europhysics 93 Conference, Marseille, France, 1993 and DELPHI 94-32 CAL 113, 1994.

[5] A.C. Benvenuti et al., STIC, The New DELPHI Luminosity Monitor, presented by A. Maio, contribution to the International Conference on Calorimetry, La Biodola, Italy, 1993 and DELPHI 94-31 CAL 112, 1994.

[6] B. Loher, S. Weissenrieder, F. Barreiro and E. Ros, An Electromagnetic Calorimeter with Wavelength Shifting Readout, Nucl. Instr and Meth. A254 (1987) 26;
H. Fessler et al., A Scintillator-Lead Photon Calorimeter Using Optical Fiber Readout Systems, Nucl. Instr. and Meth. A240 (1985) 284;
G. S. Atoyan et al., A Lead-Scintillator Electromagnetic Calorimeter with Wavelength Shifting Fiber Readout, Nucl. Instr and Meth. A320 (1992) 144;

[7] R. Turlay, Physics at LEP200, DPhPE 87-18, November, 1987;
The DELPHI Collaboration, Report from the Working Group on LEP200 Physics, DELPHI 92-166 PHYS 250 (1992);
J.-E. Augustin, Physics at LEP 200, LAL 91-74, December 1991;
D. Treille, The LEP 200 Programme, CERN-PPE/93-54/REV., 26 March 1993;

[8] M. Laakso et al.,Operation and Radiation Resistance of a FOXFET Biasing Structure for Silicon Strip Detector, NIM A326 (1993) 214-221.

[9] S.J. Alvsvaag et al., The Silicon Shower Maximum Detector for the STIC, presented by M. Prest, contribution to the 6th Pisa Conference on Advanced Detectors, Isola d'Elba,Italy, May 21-26, 1994, and DELPHI 94-126 CAL 117;

[10] M. Bonesini et al., Simulation of the DELPHI STIC Calorimeter, DELPHI 93-118 CAL 108, October 1993;

[11] G. Della Ricca, STIC: Il nuovo Monitor di Luminosità di DELPHI, Diploma Thesis, Università di Trieste, 10 Dec., 1993;

[12] R. Brun et al., GEANT3, DD/ EE/ 81-1, CERN 1987;
GEANT, Detector Description and Simulation Tool, CERN Program Library Long Writeup W5013, March 1994;

[13] W.R. Nelson et al., EGS4 User Manual, SLAC-265, SLAC Publications Office (1985);

[14] A. De Angelis, Three-dimensional parameterization of photon-initiated high energy showers, Nucl. Instr and Meth. A271 (1988) 455-463;

[15] E. Belau et al., Charge Collection in Silicon Strip Detectors, Nucl. Instr. and Meth. 214 (1983) 253-260;

[16] M. Koratzinos, VSAT Position Reconstruction, University of Torino, Aug. 1991;

[17] E. Heijne, P. Jarron, Silicon Microstrip Detectors, a New Tool for High Energy Physics, CERN/EF 81-16, 15 December 1981;

[18] F. Lemeilleur et al., Lateral Electromagnetic Shower Development in Si/W and Si/U Sandwich Calorimeter, IEEE Trans. Nucl. Sci. vol NS-34, 1, Feb. 1987;

[19] P. G. Rancoita, A. Seidman, Silicon Detectors in Electromagnetic and Hadronic Calorimetry, Nucl. Instr and Meth. A263 (1988) 84-93;

[20] E. Longo, I. Sestili, Nucl. Instr. Meth. 128 (1975);

[21] M. Huhtinen, Delta Ray Effects in Silicon Strip Detectors, HU-SEFT-R, 92-06;

[22] B. Rossi, K. Greisen, Cosmic Ray Theory, Rev. Mod. Phys. 13 (1941) 240;
B. Rossi, High Energy Particles, Prentice-Hall, New York, (1952).